


RESEARCH ARTICLE

Open Access



# Unveiling a novel memory center in human brain: neurochemical identification of the *nucleus incertus*, a key pontine locus implicated in stress and neuropathology

Camila de Ávila<sup>1\*</sup> , Anna Gugula<sup>2†</sup>, Aleksandra Trenk<sup>2†</sup>, Anthony J. Intorcchia<sup>3,4</sup>, Crystal Suazo<sup>1</sup>, Jennifer Nolz<sup>1</sup>, Julie Plamondon<sup>5</sup>, Divyanshi Khatri<sup>1</sup>, Lauren Tallant<sup>6</sup>, Alexandre Caron<sup>5,7</sup>, Anna Blasiak<sup>2</sup>, Geidy E. Serrano<sup>3,4</sup>, Thomas G. Beach<sup>3,4</sup>, Andrew L. Gundlach<sup>8</sup> and Diego F. Mastroeni<sup>1,3</sup>

## Abstract

**Background** The *nucleus incertus* (NI) was originally described by Streeter in 1903, as a midline region in the floor of the fourth ventricle of the human brain with an ‘unknown’ function. More than a century later, the neuroanatomy of the NI has been described in lower vertebrates, but not in humans. Therefore, we examined the neurochemical anatomy of the human NI using markers, including the neuropeptide, relaxin-3 (RLN3), and began to explore the distribution of the NI-related RLN3 innervation of the hippocampus.

**Methods** Histochemical staining of serial, coronal sections of control human postmortem pons was conducted to reveal the presence of the NI by detection of immunoreactivity (IR) for the neuronal markers, microtubule-associated protein-2 (MAP2), glutamic acid dehydrogenase (GAD)-65/67 and corticotrophin-releasing hormone receptor 1 (CRHR1), and RLN3, which is highly expressed in NI neurons in diverse species. *RLN3* and vesicular GABA transporter 1 (*vGAT1*) mRNA were detected by fluorescent in situ hybridization. Pons sections containing the NI from an AD case were immunostained for phosphorylated-tau, to explore potential relevance to neurodegenerative diseases. Lastly, sections of the human hippocampus were stained to detect RLN3-IR and somatostatin (SST)-IR.

**Results** In the dorsal, anterior-medial region of the human pons, neurons containing RLN3- and MAP2-IR, and *RLN3/vGAT1* mRNA-positive neurons were observed in an anatomical pattern consistent with that of the NI in other species. GAD65/67- and CRHR1-immunopositive neurons were also detected within this area. Furthermore, RLN3- and AT8-IR were co-localized within NI neurons of an AD subject. Lastly, RLN3-IR was detected in neurons within the CA1, CA2, CA3 and DG areas of the hippocampus, in the absence of *RLN3* mRNA. In the DG, RLN3- and SST-IR were co-localized in a small population of neurons.

**Conclusions** Aspects of the anatomy of the human NI are shared across species, including a population of stress-responsive, RLN3-expressing neurons and a RLN3 innervation of the hippocampus. Accumulation

<sup>†</sup>Anna Gugula and Aleksandra Trenk contributed equally.

\*Correspondence:

Camila de Ávila  
cdeavila@asu.edu

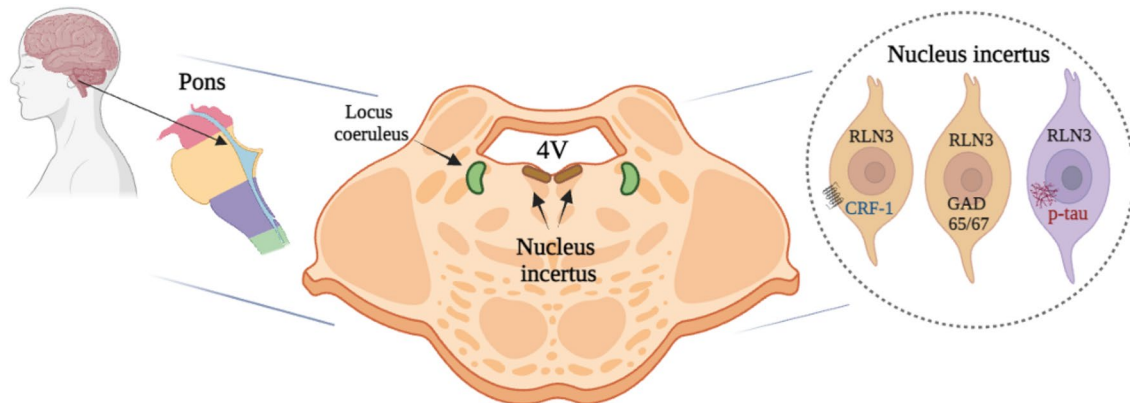
Full list of author information is available at the end of the article



of phosphorylated-tau in the NI suggests its possible involvement in AD pathology. Further characterization of the neurochemistry of the human NI will increase our understanding of its functional role in health and disease.

**Keywords** Brainstem, Dementia, Hippocampus, Human, Memory, Nucleus incertus, Relaxin-3

### Graphical Abstract



### Background

The brainstem receives a range of sensory and autonomic inputs from the periphery and the spinal cord, and neurons in this region project throughout the brain to distribute these integrated signals to influence multiple higher-processing networks. Ascending networks including the locus coeruleus (LC) and medullary raphe nuclei are highly susceptible to neurodegenerative diseases, including Alzheimer's disease (AD) [1–4]. In addition, extensive studies of the LC have contributed to understanding the involvement of the hippocampus in memory [5–7].

The brainstem nucleus incertus (NI) or the 'uncertain nucleus', was originally described by anatomist, George L. Streeter in 1903 as a midline region in the floor of the fourth ventricle (4V) of the human brain with 'unknown' function [8]. An equivalent area was also described in guinea pig (1923) [9], hamster (1954) [10], and cat (1968) [11]. Thereafter, many decades later, a large majority of neurons in the rat NI or *nucleus O* [12] were shown to express the inhibitory neurotransmitter,  $\gamma$ -aminobutyric acid (GABA), as reflected by staining against the GABA-synthesizing enzyme, glutamic acid dehydrogenase (GAD), and in situ hybridization (ISH) for *vGAT1* mRNA [13, 14]. Since then, the neuroanatomy of the NI and its connections throughout the brain has been systematically mapped using various histological methods, in rats [14–19], mice [20–24], zebrafish [25], and in non-human primate [26], but not in humans.

In general, the NI is a bilateral nucleus, located in the midline adjacent to the more lateral LC [15, 17, 22, 24]. Its anatomy varies slightly in different species. In adult rats, the NI extends for ~0.7 mm from Bregma – 9.12 mm to Bregma – 9.84 mm and it is referred to as 'nucleus O' by Paxinos and Watson [12, 17, 19]. In mice, the NI is located more ventral to the 4V than in rats, in the midline central gray of the dorsal pons [22]. In the macaque, the NI is located adjacent to the 4V, within the ventromedial central gray of the pons/medulla, and medial to the LC [26].

Recent research has identified specific neuroanatomical and functional connections between the NI and the septohippocampal system (SHS) and demonstrated that the NI plays a role in spatial and contextual fear memory [14, 21, 23, 27, 28]. The predominant inhibitory neurotransmitter system (i.e., GABAergic system) is associated with bi-directional projections between the NI and SHS [29, 30], and these NI-related circuits can regulate fear memory via effects on SST-positive interneurons in the hippocampus and hippocampally-projecting septal neurons [21, 23]. In addition, the degeneration of GABA and SST/GABA neurons occurs in the medial SHS and basal forebrain cortical systems in AD and other neurodegenerative dementia [31, 32].

Importantly, a major population of NI neurons has been demonstrated to produce relaxin-3 (RLN3) in multiple species [24, 26, 33, 34]. RLN3 is a highly-conserved neuropeptide [35, 36] that signals via the relaxin-family

**Table 1** Clinical and pathological characteristics of studied cases for each anatomical region and technique used

Tissue	Technique			Subjects						
	IHC	IF	ISH	Group	Race	Sex	Age	PMI (h)	APOE	Braak
Hemi-pons	X	X		CT	W	M	75	2	3/3	III
				CT	W	F	71	2.88	3/3	IV
			X	AD	W	M	81	3	3/4	V
Full pons	X			CT	W	F	96	3.52	3/3	IV
Hippocampus	X	X		CT	W	F	60	3.67	3/3	I
			X	CT	W	F	59	3.15	3/3	I
Testis	X			CT	W	M	97	8.53	3/3	IV

AD, Alzheimer's disease; CT, control without history of dementia and neurological disorders; IHC, immunohistochemistry; F, female; IF, immunofluorescence; ISH, in situ hybridization; M, male; PMI, post-mortem interval in hours; W, white

peptide-3 receptor (RXFP3) [24, 37, 38]. RLN3/RXFP3 signaling is strategically positioned to modulate SHS-related learning and memory processes that are integral in AD symptomology [30, 39, 40]. In addition, NI is a stress-responsive region and its neurons express receptors for the stress hormone, corticotropin-releasing hormone (CRH) [41–43]. Thus, in light of the likely importance of the NI and associated GABAergic and neuropeptide systems in memory and key sensory and autonomic processes in humans under different physiological conditions, it is timely to investigate the neurochemical anatomy of human NI neurons.

## Methods

### Postmortem human tissue

The postmortem human brain tissue used in this study was fully characterized and generously provided by the Arizona Alzheimer Disease Research Center (ADRC) Pathology Core, Banner Sun Health Research Institute, Brain and Body Donation Program (BBDP, Sun City, AZ, USA, <http://www.brainandbodydonationprogram.org>). Autopsy and tissue fixation were conducted as described [44]. Details for each subject are provided in Table 1.

### Multiplex fluorescence in situ hybridization

Expression of *RLN3* and *vGAT1* mRNA in postmortem human pons and hippocampus (from control subjects; see Table 1) was assessed using RNAscope™ Multiplex Fluorescent ISH (Advanced Cell Diagnostics (ACD), Hayward, CA, USA). Briefly, fresh-frozen, coronal sections (10 µm) were cut at – 20 °C using a cryostat, and mounted onto Superfrost-Plus slides, according to the BBDP protocol [44]. All procedures were conducted following the user manual for RNAscope™ Multiplex Fluorescent V2 assay (fresh-frozen sections) provided by the manufacturer (ACD). The slides were stored at – 80 °C until a 1 h fixation in a freshly prepared solution of 4% formaldehyde in phosphate-buffered saline (PBS, pH

7.4, initially 4 °C) at room temperature (RT), followed by washing in PBS and dehydration in ethanol solutions of increasing concentration (50, 70, and 100%). Dehydrated sections were stored at – 20 °C for 48 h and then air-dried, outlined with Immedge Hydrophobic Barrier Pen (Vector Laboratories, Burlingame, California, USA), incubated with hydrogen peroxide for 10 min at RT, and washed in distilled water. Next, after applying protease IV pre-treatment solution (ACD) for 30 min at RT and washing in PBS, the sections were hybridized for 2 h at 40 °C with a solution of multiplex probes for: *RLN3* (Hs-RLN3-C1, Cat. No. 590151, ACD) and vesicular GABA transporter 1 (*vGAT1*, Hs-SLC32A1-C3, Cat. No. 415681-C3, ACD). Sections were washed in 1 × Wash Buffer (ACD) between every hybridization step. Following all amplification steps, HRP-C1 (labelled with TSA Vivid Fluorophore 650, 1:1,000, Cat. No. 7536, in TSA buffer, ACD) and HRP-C3 (labelled with TSA Vivid Fluorophore 570, 1:1,000, Cat. No. 7535, in TSA buffer, ACD) signal was developed. Finally, the tissue was counterstained with DAPI, coverslipped with ProLong Gold antifade reagent (Invitrogen, Thermo Fisher Scientific, Life Technologies Corporation, Eugene, OR, USA) and imaged using an Axio Imager M2 fluorescence microscope (Zeiss) with an automatic stage and AxioCam 503 mono camera (Zeiss). 20 × /0.5 EC Plan Neo-Fluar objective was used for acquisition of panoramic z-stack images of the NI and the hippocampus areas (scaling: 0.227 µm in x and y, and 1.250 µm in z axis) and 40 × /1.3 Oil EC Plan Neofluar objective for obtaining single representative z-stack images of NI neurons (scaling: 0.114 µm in x and y, and 0.280 µm in z).

The images were then processed in Zen software (3.3 blue edition and 2.3 SP1 black edition, Zeiss) and ImageJ [45] to improve the signal-to-noise ratio and converted into maximum intensity projection images.

### Immunohistochemistry (IHC)

Chromogenic immunohistochemical studies were completed using sections from human pons, hippocampus, and testis (see Table 1). Tissue was fixed according to the BBDP protocol [44], sectioned at 30–40  $\mu\text{m}$  on a microtome, and mounted on charged glass slides for histology. Briefly, free-floating sections were blocked in 1%  $\text{H}_2\text{O}_2$  and 3% bovine serum albumin (BSA, Cat. No. D5637, Sigma-Aldrich, St. Louis, Missouri, USA). Pons sections were stained with hematoxylin and eosin (H&E, Cat. No. 26041-06, EMS, Hatfield, PA, USA and Cat. No. E511-100, Thermo Fisher Scientific, Tempe, AZ, USA). Sequential sections were incubated in antisera raised against microtubule-associated protein-2 (MAP2, 1:8,000, Cat. No. ab183830, anti-rabbit, Abcam, Fremont, CA, USA) or RLN3 (1:1,500, Cat. No. PA47448, anti-goat, Invitrogen, Carlsbad, CA, USA), overnight (ON) at 4 °C. Sections were washed and then incubated in species-specific secondary antisera (1:1,000 Cat. No. Vector BA-1000, goat anti-rabbit IgG (H+L), biotinylated, Vector Laboratories Inc., Burlingame, California, USA, or Cat. No. Vector BA-5000, rabbit anti-goat IgG (H+L), biotinylated, Vector Laboratories Inc., Newark, California, USA) for 2 h at RT. Sections were washed and incubated in 1:1,000 avidin/biotin reagent (VECTASTAIN ABC-HRP Kit (Standard), Cat. No. PK-4000, Vector Laboratories Inc., Burlingame, California, USA), washed and incubated in 3,3'-diaminobenzidine (DAB, Cat. No. D5637, Sigma-Aldrich, St. Louis, Missouri, USA; concentrated: 10 mg/mL). Sections were reacted for 10 min (MAP2) and 30 min (RLN3), dried, dehydrated through graded alcohols, cleared in xylene, and mounted using Permount (Cat. No. 17986-01, EMS, Hatfield, PA USA). Hippocampus and testis sections were only incubated with RLN3 antibody and subjected to the same steps described above.

### Image analysis

Imaging of tissue sections stained using immunohistochemistry was performed using an Olympus IX70 microscope equipped with brightfield illumination (Olympus, Tokyo, Japan). Results were captured using an Olympus DP-71 color digital camera. Whole slide images were acquired using an Olympus VS200 slide scanner and processed using Olympus DESKTOP v3.4.1 to generate representative images.

### Immunofluorescence

Postmortem brain samples were selected to best match critical factors such as postmortem interval (PMI), age and sex, as well as other relevant covariates (Table 1). Sections were washed (3 $\times$ ) in phosphate-buffered saline with 0.1% Tween<sup>®</sup> 20 detergent (PBS-T, Cat. No.

20012-027, GIBCO PBS pH 7.2 (1X), Life Technologies Corporation, Grand Island, New York, USA, with Tween<sup>®</sup> 20 detergent, Cat. No. P1379, Sigma Aldrich Company, St. Louis, Missouri, USA), and blocked with 3% BSA, with incubation for 1 h. After further washing, sections were incubated in a range of combined primary antisera [RLN3 (1:1,500, Cat. No. PA47448, anti-goat, Invitrogen, Carlsbad, CA, USA) and AT8 (1:500, MN1020, anti-mouse, Invitrogen, Carlsbad, CA, USA), or corticotrophin-releasing hormone receptor 1 (CRHR1, 1:500, Cat. No. ab150561, anti-rabbit, Abcam, Fremont, CA, USA), or GAD65/67 (1:500, Cat. No. PA5-104543, anti-rabbit, Invitrogen, Carlsbad, CA, USA), or MAP2 (1:500, Cat. No. ab183830, anti-rabbit, Abcam, Fremont, CA, USA), or SST (1:200, Cat. No. ab108456, anti-rabbit, Abcam, Fremont, CA, USA)] antisera; ON at 4 °C.

Sections were washed 3 $\times$  in PBS-T and incubated in species-specific, fluorophore-conjugated secondary antibodies (1:1000, Red: Cat. No. A11036, AlexaFluor 568 goat anti-rabbit IgG (H+L) 2 mg/mL, and 1:1,000, Green: Cat. No. A11034, AlexaFluor 488 goat anti-rabbit IgG (H+L) 2 mg/mL, or Cat. No. A11055, donkey anti-goat IgG (H+L) 2 mg/mL, or Cat. No. A11029, goat anti-mouse IgG (H+L) 2 mg/mL, Life Technologies, Eugene, OR, USA). After a final wash, sections were mounted, dipped in 1% Sudan Black (Cat. No. 199664, Sigma-Aldrich, St. Louis, Missouri, USA) to reduce autofluorescence, and coverslipped with UltraCruz containing DAPI (UltraCruz<sup>®</sup> Hard-set mounting medium, sc-359850, Dallas, TX, USA).

### Imaging analysis

Imaging of tissue sections stained with fluorescent markers was performed using an Olympus IX70 microscope equipped with epifluorescence illumination. Images were captured using an Olympus DP-71 color digital camera. High-resolution micrographs were acquired using a Leica SP8 confocal microscope (Leica, Wetzlar, Germany).

### Specificity of RLN3 antiserum—Dot blot and pre-adsorption tests

Dot blot analysis was used to test the specificity of the polyclonal RLN3 antibody used in the immunohistochemical studies for recognizing human RLN3 peptide. Lyophilized human RLN3 (Cat. No. 035–36, Phoenix Pharmaceuticals, Burlingame, CA, USA) was reconstituted in distilled water and was used at a concentration of 10  $\mu\text{g}$ . Two  $\mu\text{l}$  of RLN3 peptide were added to the center of a 0.2  $\mu\text{m}$  nitrocellulose membrane (Cat. No.1620146, Bio-Rad, Hercules, CA, USA). Non-specific sites were blocked by incubation with 5% BSA in Tris-buffered saline with 0.1% Tween<sup>®</sup> 20 detergent (TBS-T, 20 mM Tris-HCl and 150 mM NaCl, Sigma-Aldrich, Cat. Nos.



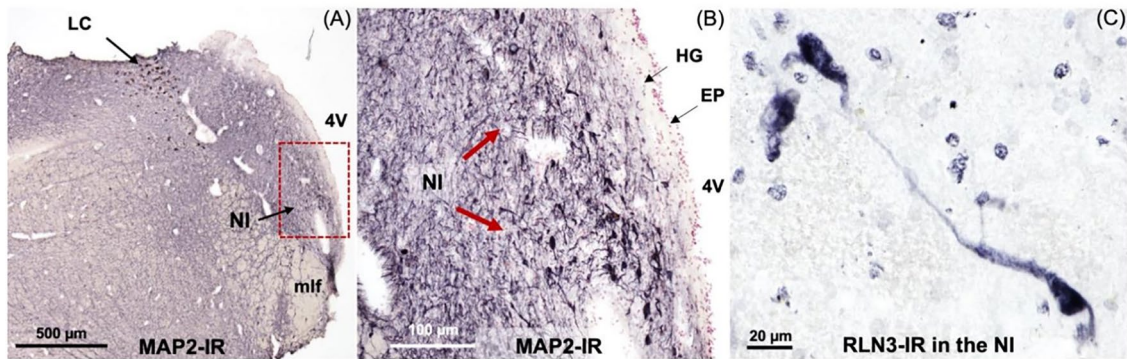


**Fig. 1** RLN3-Immunoreactivity in the coronal anterior hemi-pons of human brain. **A** Neuronal populations in the human pons, stained for MAP2-IR. MAP2 is a marker of neuronal cells, their perikarya and dendrites [94]. **B** A higher magnification view of the human pons, with red arrows indicating MAP2-IR neurons in an area adjacent to the medial longitudinal fasciculus equivalent to that containing RLN3-positive NI neurons in the macaque. **C** RLN3-immunopositive neurons in human NI. Abbreviations: EP, ependyma, 4V, fourth ventricle, HG, Hypocellular gap, IR, immunoreactivity, LC, locus coeruleus, MAP2, microtubule-associated protein-2, mlf, medial longitudinal fasciculus, NI, *nucleus incertus*

T5941, T1503, S3014, with Tween® 20 detergent, Sigma Aldrich, Cat. No. P1379, St. Louis, Missouri, USA) for 1 h at RT, and then the membrane was incubated with RLN3 antiserum (1:15,000, Cat. No. PA47448, anti-goat, Invitrogen, Carlsbad, CA, USA) for 30 min. The membrane was washed  $3 \times 10$  min in TBS-T, incubated with a secondary antibody conjugated with HRP (1:500, Cat. No. PI-9500, Horse Anti-Goat IgG (H+L), peroxidase; Vector Laboratories Inc., Newark, CA, USA) for 30 min at RT, then washed  $3 \times 10$  min in TBS-T and  $1 \times 5$  min in TBS. The membrane was incubated with ECL reagent for 1 min, then imaged on an Amersham Imager 680 (GE), with an exposure time of 90 s.

Validation of the dot blot result was also performed using a pre-adsorption assay. An aliquot of RLN3 antiserum (see details in IHC section) was pre-incubated ON with RLN3 peptide (molar ratio 1:10 antibody:peptide). RLN3 immunohistochemistry was repeated as described above in  $40 \mu\text{m}$ , free-floating sections from postmortem human testis (a positive control tissue for RLN3 peptide expression [46]).

## Results

In this study, we identified the NI of the human brain, in postmortem tissue using RLN3, MAP2, GAD 65/67, and CRHR1 as neurochemical markers for the area. Combining techniques that preserve the neuroanatomy—ISH and IHC—we first detected the presence of *RLN3* mRNA and peptide in the human NI, using hemi-brain sections. The neuronal distribution within the dorsal pons at the level of the NI was first mapped using an antibody for MAP2, which is expressed in neurons [47] (Fig. 1A, B). Multiple neuronal populations were stained for MAP2, in the dorsal, anterior-medial region of the pons; the area adjacent to the 4V and dorsal to the medial longitudinal fasciculus

(mlf); and the distribution was similar to the distribution of neurons in the area of macaque brain identified as the NI [26]. Once a neuronal population at the anticipated rostrocaudal level of the human NI was identified, RLN3-IR was detected to confirm the location and better define the anatomical boundaries of the NI (Fig. 1C). The presence of *RLN3* mRNA was detected to investigate whether RLN3 translation was also occurring within the NI (Fig. 2A). *RLN3* mRNA and peptide were confirmed within the antero-medial level of the pons. Importantly, as in other species tested [37], ISH results indicated that *RLN3* mRNA is colocalized with *vGAT1* mRNA in human NI (Fig. 2B, C), which indicates the GABAergic nature of NI neurons synthesizing RLN3 in the human brain. In line with findings in rats [17, 20], and to some extent in mice [20, 24], the anatomy of the NI in humans was characterized by a compact and more dispersed regions. Previous reports in the rat brain [17] indicated that the *pars compacta* displayed a dense population of neurons near the 4V, while the *pars dissipata* contained fewer, more sparse neurons along the superior part of the mlf.

We validated the specificity of the RLN3 antisera for detection of human RLN3 using sections of postmortem human testis (positive control) [46] incubated with or without RLN3 antiserum subjected to pre-adsorption of the native peptide (Supplementary Fig. 1A–F). The pre-adsorption completely abolished specific immunostaining. In addition, a dot blot experiment demonstrated that the RLN3 antiserum binds to native RLN3 peptide (Supplementary Fig. 1G), although we did not assess its cross-reactivity with other related or unrelated peptides. In studies to confirm the neuronal nature of RLN3 immunopositive cells, we co-incubated RLN3 and MAP2 antisera (Fig. 3) and immunofluorescent detection revealed consistent colocalization of these markers within neurons in

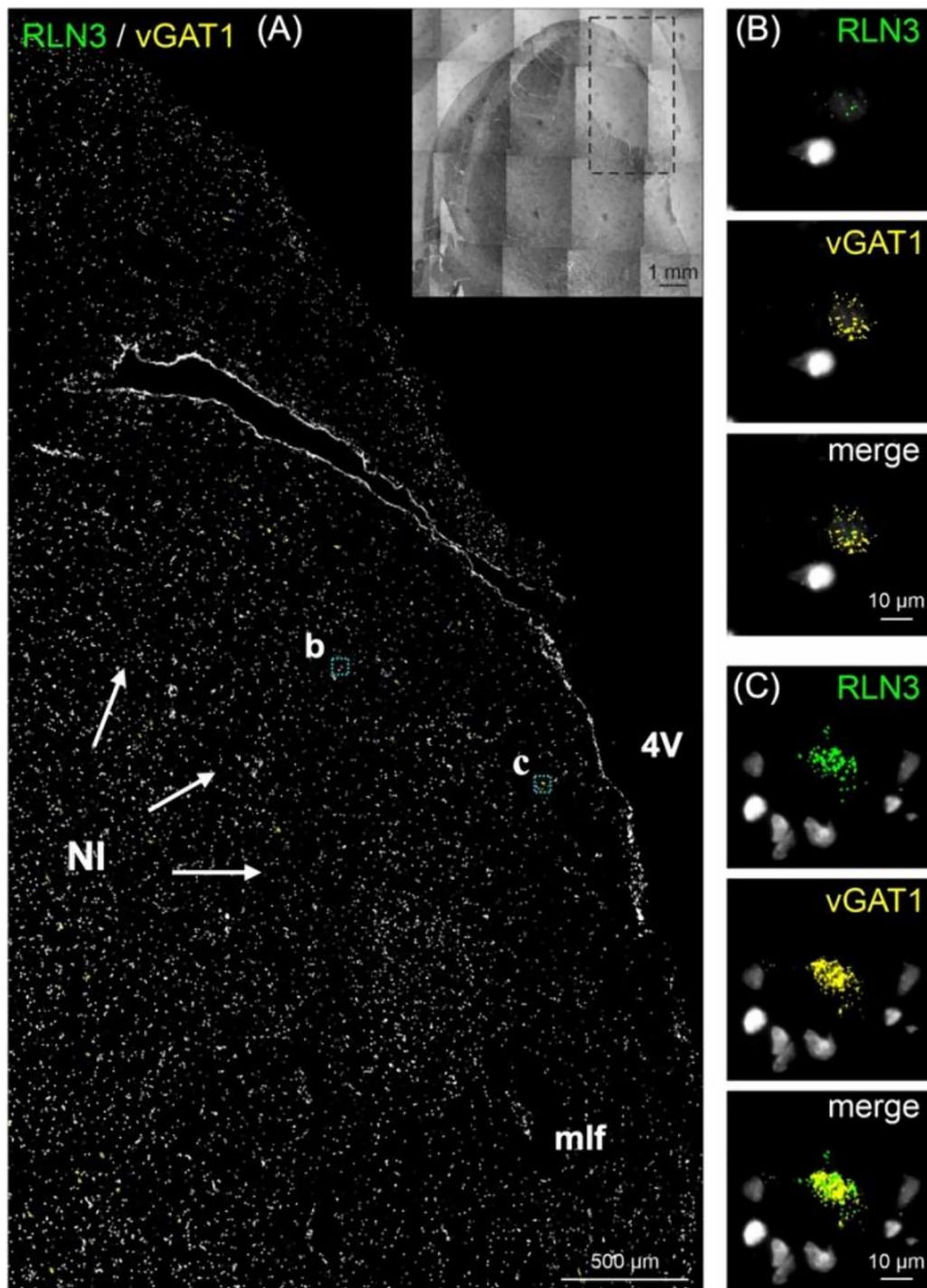


**Fig. 2** In situ hybridization of *RLN3* mRNA in the NI. **A** *RLN3* mRNA detection in coronal anterior hemi-pons of the human brain. **B** Higher magnification images of *RLN3* mRNA (green particles) and **C** *vGAT1* mRNA (yellow particles) co-localized in neurons in the NI area (merge). Inset represents the hemi-pons section under brightfield illumination. Abbreviations: 4V, fourth ventricle, mlf, medial longitudinal fasciculus, NI, *nucleus incertus*, *vGAT1*, vesicular GABA transporter-1



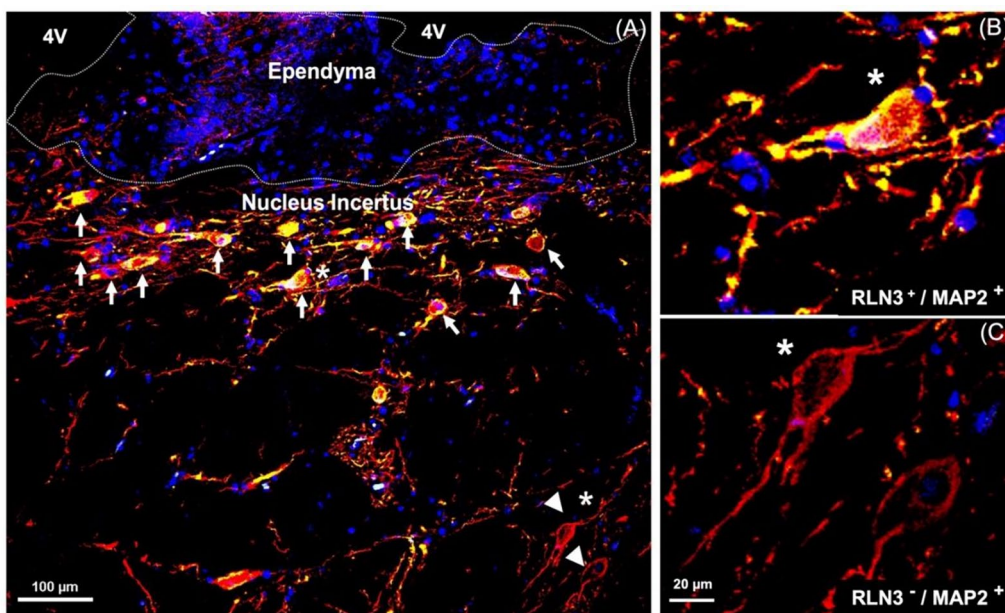


**Fig. 3** RLN3-immunoreactivity in neurons containing Microtubule-Associated Protein-2, a marker of neuronal cells, their perikarya, and dendrites [94]. **A** NI in human brain; white arrows indicate RLN3-immunoreactivity co-localized with MAP2. **B** Higher magnification view of a RLN3<sup>+</sup>/MAP2<sup>+</sup> neuron indicated with a white star. **C** Higher magnification of RLN3<sup>-</sup>/MAP2<sup>+</sup> neurons indicated in A with white arrowheads. MAP2 (red), RLN3 merging with MAP2 (yellow), DAPI (blue). Abbreviations: 4V, fourth ventricle, MAP2, microtubule-associated protein 2, RLN3, relaxin-3

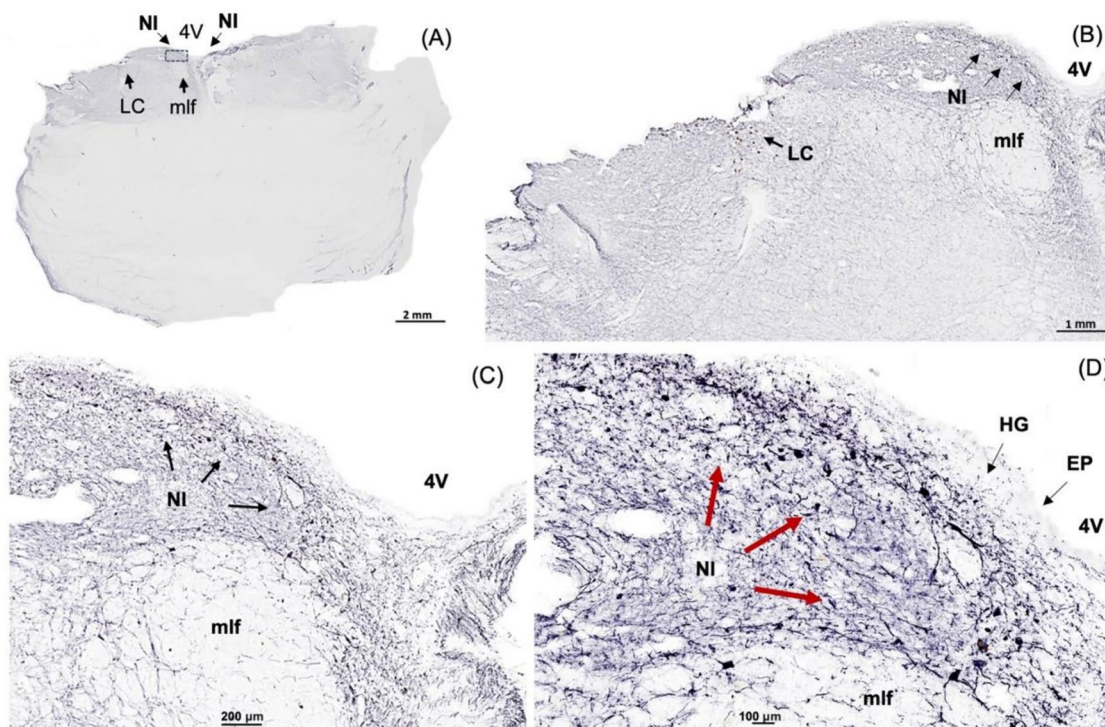


**Fig. 4** MAP2-immunoreactivity in neurons in the coronal anterior pons. **A** Low-power image of the neuroanatomy of the human pons containing the NI stained for MAP2-IR, a marker of neuronal perikarya and dendrites [94]. **B** Higher magnification image of the boxed area in A. **C** Higher magnification of the NI area in B. **D** Higher magnification of the NI area in C. Abbreviations: EP, ependyma, HG, hypocellular gap, IR, immunoreactivity, LC, locus coeruleus, MAP2, microtubule-associated protein-2, mlf, medial longitudinal fasciculus, NI, nucleus incertus, 4V, fourth ventricle

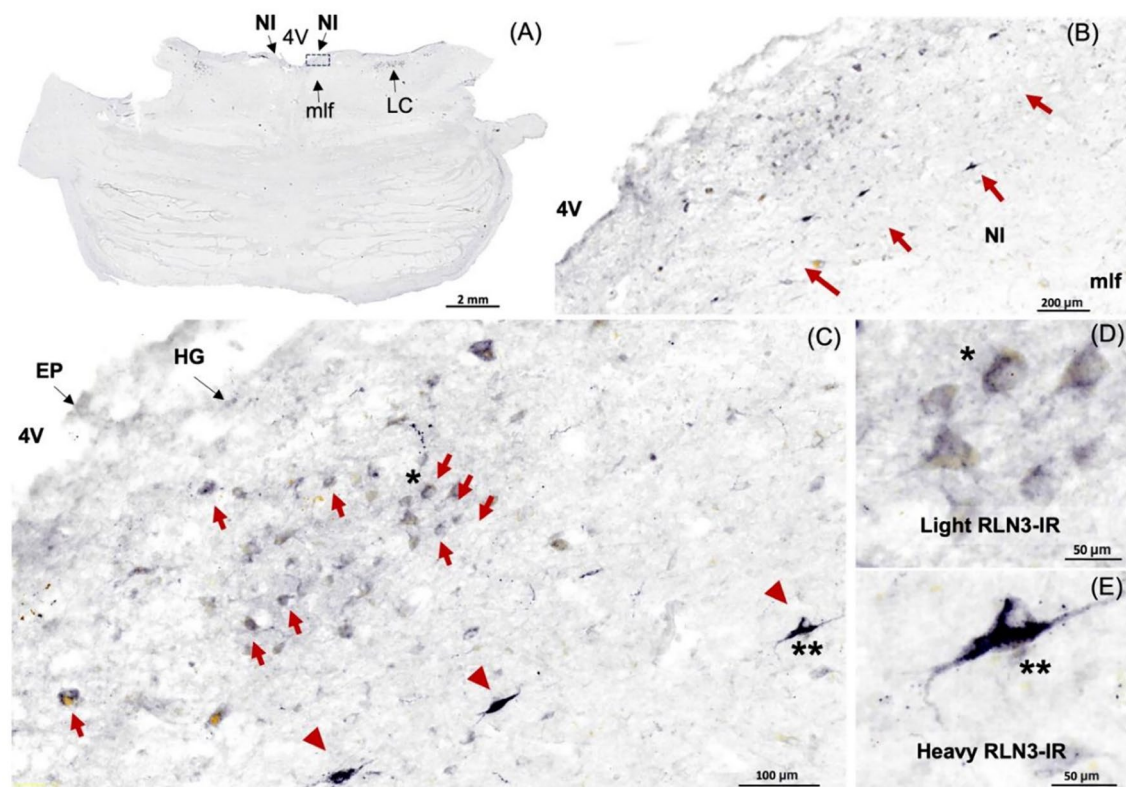


**Fig. 5** RLN3-Immunoreactivity in the coronal human NI. **A** Low power image of the anterior level of the pons, with the NI located at the floor of the 4V, above the mlf and lateral to the LC. **B** Higher magnification image of the boxed area in **A**. **C** Higher magnification image of the boxed area in **B**, with neurons lightly and heavily stained for RLN3 indicated by red arrows and red arrowheads, respectively. **D**, **E** Higher magnification images of neurons with light and heavy staining for RLN3-IR, respectively. Abbreviations: EP, ependyma, 4V, fourth ventricle, HG, Hypocellular gap, IR, immunoreactivity, LC, locus coeruleus, mlf, medial longitudinal fasciculus, NI, *nucleus incertus*

the NI region, while in areas outside the NI, MAP2 positive neurons were negative for RLN3-IR (Fig. 3).

After identifying the human NI region in sections of hemi-brain samples and validating the ability of the RLN3 antiserum to recognize the native peptide, we conducted further experiments in sections of intact, bilateral pons and immunostained them for additional markers. We confirmed the distribution of MAP2-containing neurons in the same NI area identified using hemi-pons sections (Fig. 4), and detected nuclear and cytoplasmic structures using H&E (Supplementary Fig. 2). The presence of the NI bilaterally was revealed by detection of RLN3-IR (Fig. 5), and different (light/heavy) staining of the peptide was observed in different neurons within the area (Fig. 5D, E).

Additional immunostaining was completed to further verify possible similarities in the neurochemistry of the human NI with other species. In all non-human species examined (i.e., rats, mice, macaque), RLN3-positive neurons are GABAergic [14, 33] and express the CRHR1 in the rat [34, 48]. GAD65/67- and CRHR1-IR were detected in the human NI (Fig. 6), and both CRHR1- and

GAD65/67-IR were co-localized with RLN3-IR (Fig. 6C, F).

In light of the possible association between the NI neural network and memory and cognition under normal and pathological conditions [21, 23, 39, 40], we examined the relationship between a marker for AD-related pathology, phosphorylated-tau and RLN3-expressing neurons in the NI from an AD subject (Fig. 7). Notably, phosphorylated-tau was detected at the NI level of pons sections from an AD subject, as reflected by AT8-IR and these neurons also contained RLN3-IR (Fig. 7C), whereas no AT8-IR was detected in NI neurons of a control subject (Fig. 7D). Successful detection of AT8-IR in LC of AD sections was used as a positive control for the antibody (data not shown).

Lastly, we conducted initial studies of the presence of NI-related RLN3-IR, in postmortem sections of hippocampus from a control subject, and observed a distinct accumulation of RLN3-IR in sparse neurons in the CA1-2 and CA3/DG layers (Fig. 8). Notably, RLN3 mRNA was not detected within the hippocampus (data not shown), indicating likely peptide accumulation in the area.



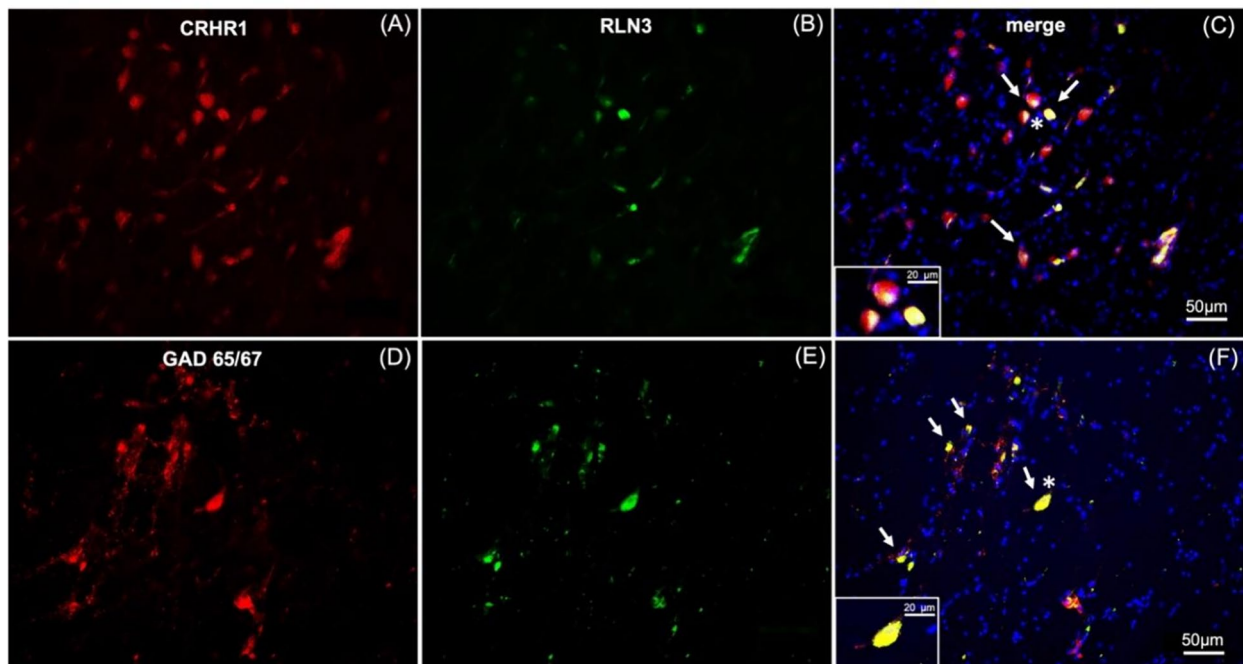


**Fig. 6** RLN3-immunoreactive neurons in the NI co-express CRHR1- and GAD65/67-immunoreactivity. **A–C** RLN3 positive neurons and surrounding cells in the coronal human NI region, co-express corticotropin-releasing hormone receptor-1 immunoreactivity (CRHR1; white arrows). **D–F** RLN3 positive neurons co-express glutamic acid decarboxylase 65/67 immunoreactivity (GAD65/67, white arrows). Insets represent higher magnification images of neurons indicated by an asterisk in **C** and **F**. CRHR1 and GAD65/67 (red), RLN3 (green), DAPI (blue), merged image (yellow)

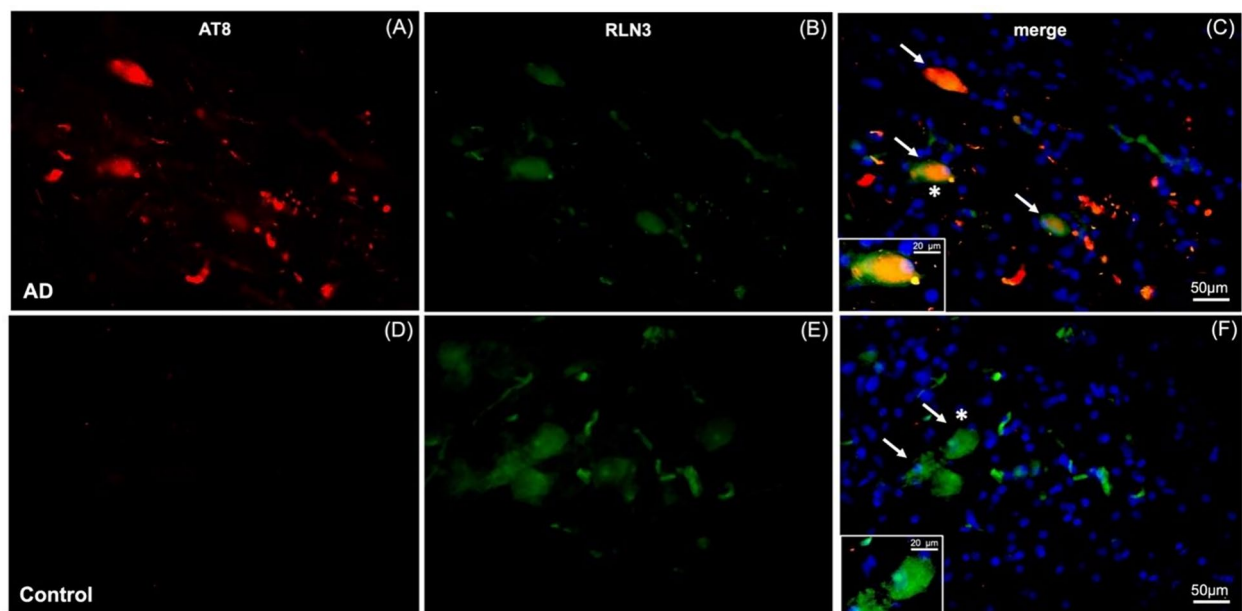


**Fig. 7** NFT co-localized with RLN3-immunoreactivity in the NI of AD brain. **A–C** AT8 (a marker for neurofibrillary tangles, NFT) and RLN3 positive staining of neurons in the coronal human NI of an AD case, with co-expression of RLN3 and NFT (indicated by white arrows). **D–F** AT8 and RLN3 staining of the NI of a control, age and sex-matched, non-demented subject. Insets in **C** and **F** represent higher magnification images of neurons marked with an asterisk, and reveal the co-localization of NFT and RLN3 in AD but not control brain. AT8 (red), RLN3 (green), AT8 and RLN3 (yellow), DAPI (blue)

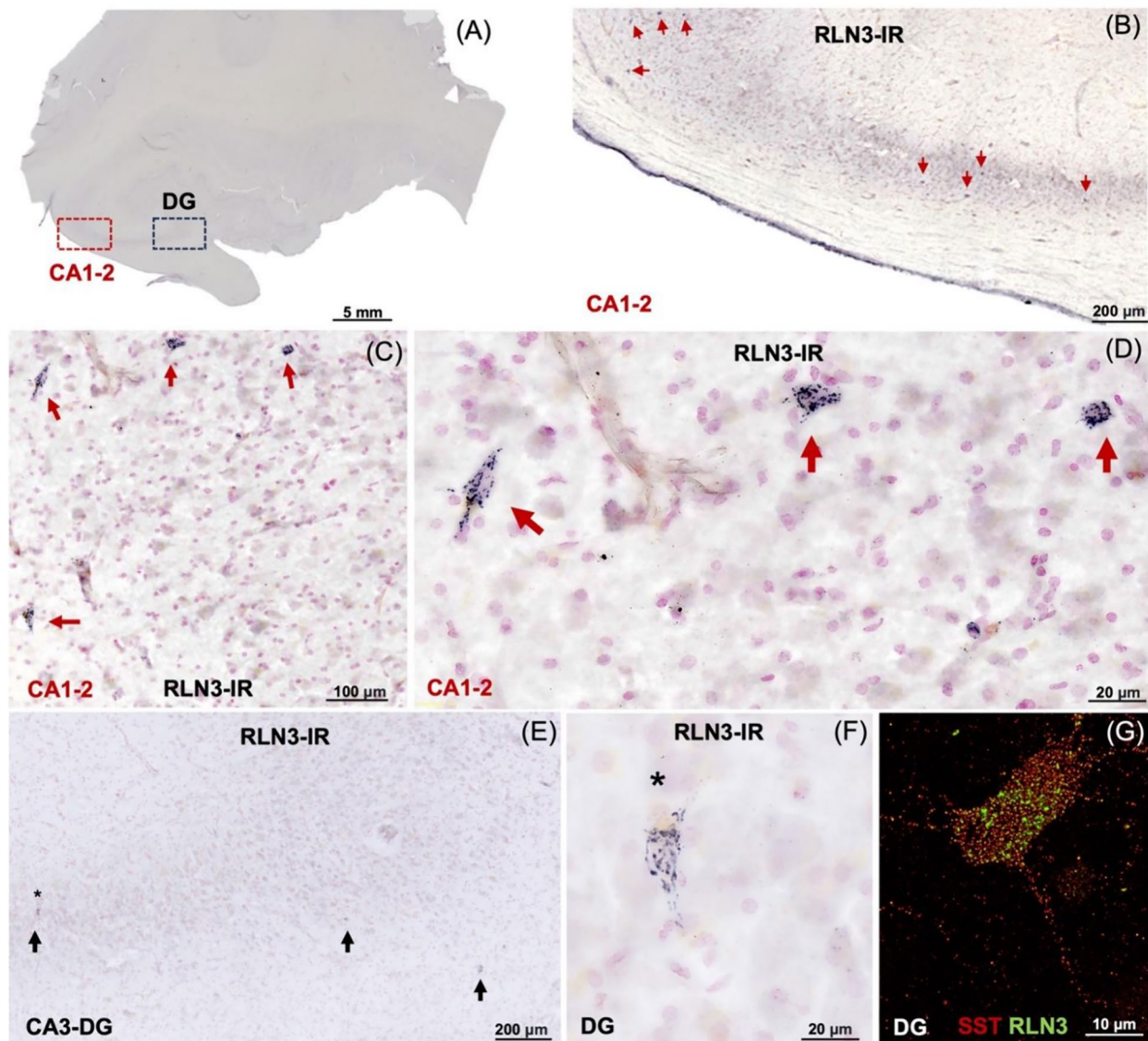


**Fig. 8** RLN3-immunoreactivity within human hippocampal neurons. **A** Overview of the neuroanatomy of the coronal hippocampus lightly counterstained with neutral red. **B–D** Higher magnification images of RLN3-immunopositive cells within the CA1-2 (red boxed area in **A**). **E, F** High magnification images of RLN3-IR in the cells within the CA3 and dentate gyrus (DG, black boxed area in **A**). **G** Interneuron within the DG labeled for RLN3-IR (green) and somatostatin-IR (SST, red). The pattern of staining suggests an accumulation of the neuropeptide on the surface of these neurons, which express the RLN3 receptor, RXP3 in mice [76]

## Discussion

The current results indicate that aspects of the anatomy and neurochemistry of the NI are preserved across species and that the human NI shares similarities with non-human primates such as the macaque [26] and common experimental species, such as rats and mice [19, 37, 49]. Marker proteins of the GABAergic and CRH-mediated stress response systems and phosphorylated-tau were detected within human RLN3 NI neurons in control and AD subjects, respectively.

Numerous earlier anatomical studies have characterized the connectivity and neurophysiological activity of the NI in rat and mouse brain, including the strong projections to the SHS system, and to multiple cortical and limbic areas involved in emotional cognition [14, 17, 18, 21], while others have characterized the nature of the transmitters, neuropeptides, and receptors expressed by different populations of NI neurons in these species [14–22], which provide an insight to the likely functional role of the NI in the human brain.

In the following sections, the significance of the current results is reviewed in the context of previous preclinical studies. It includes an overview of the existing knowledge on the role of the NI, and in particular RLN3 signaling systems, in spatial and contextual fear memory, and stress. Finally, it addresses the limitations of the current study and future experiments that are warranted based on our important initial findings.

#### Identification of the NI in human brain

In the current study, we used MAP2-IR to detect neuronal populations in an area in the human dorsomedial pontine tegmentum equivalent to that reported to contain the NI in vertebrates [17, 22, 26]. After using MAP2 to identify a neuronal population appropriately positioned adjacent to the floor of the 4V and medial to the LC, we used serial, free-floating, formalin-fixed hemibrain sections to detect the presence of RLN3, a neuropeptide marker for the NI.

#### Neurochemical profile of the NI and its functional implications

In rats and mice, RLN3 is primarily expressed in the NI [24, 34–36, 38] with some additional positive cells located in the pontine raphe nucleus (PRn), the lateroventral periaqueductal gray (PAG), and a region dorsal to the substantia nigra (SN) pars compacta [33, 34]. We observed high densities of RLN3-IR in the human NI, similar to that observed in other species [26, 50] and also detected neurons expressing a lower density of RLN3-IR. Further investigation is needed to understand whether RLN3-IR neurons in the hippocampus, might accumulate the peptide via receptor-mediated mechanisms and might display a correlation with the low RLN3-IR density observed in the NI.

RLN3 is co-expressed with GAD- and GABA-IR in GABAergic projection neurons in rats [14, 33, 51]. In humans, we also observed GAD65/67-IR co-localized with RLN3-IR and mRNA encoding the *vGAT1* co-localized with *RLN3* mRNA. In rats and mice, populations of NI neurons express other peptides, including neuromedin-B (NMB) [20] and cholecystokinin (CCK) [14, 18] and RLN3 is co-localized with NMB in the mouse [14, 22], but in a separate population to the CCK neurons in rat [14, 22]. However, unlike RLN3, which is confined to small populations of neurons in the pontine raphe, PAG, and dorso-lateral to SN [24, 33, 34], NMB and CCK are more widely expressed throughout neurons in the forebrain [52, 53]. Furthermore, multiple anatomical and pharmacological studies in the rat have revealed modulatory inputs to the NI from a range of other key neuropeptide systems, including CRH, orexin/hypocretin [54, 55] and melanin-concentrating hormone (MCH) [56], as reflected by

expression of CRHR1 [48] orexin/(hypocretin) receptors (OX1, OX2) [54, 55, 57], and MCH receptor-1 (MCH-1) [56], further reflecting the importance of the NI in the control of arousal and attention [58], processes highly related to cognition. NI neurons in rats and mice also express receptors for the monoamine transmitters, serotonin [serotonin-1A receptor (5-HT<sub>1A</sub>)] [59] and dopamine [D2-like receptor (D2R)] [14, 60]. Several of these putative influences have been explored experimentally and been found to affect the activity of rat NI neurons [19, 43, 55, 56, 60, 61]. For example, pre-clinical studies using behavioral challenges, pharmacological interventions, lesions, and electric manipulations in rats, revealed that the NI was activated by stress and is a component of the stress response/initiation circuits [24, 34, 42, 48, 62]. In the current study, CRHR1-IR was detected within human NI neurons, aligned with these pre-clinical findings [19, 34], and stress is known to affect memory at multiple points of the neuraxis [63]. In addition, anterograde tracing in mice, revealed that CRH neurons in the dorsomedial medulla innervate the NI and have been shown to regulate key aspects of sleep that drive memory consolidation [64].

In this regard, the SHS is a major target of studies aimed at understanding the etiology of age- and dementia-related memory decline; and studies in animal models have revealed that the RLN3/NI network shares anatomical similarities with other neuromodulatory networks implicated in the control of memory and arousal, and AD symptoms, such as the serotonergic, cholinergic, and noradrenergic systems [21, 65–70]. Indeed, extensive studies of the LC have contributed to understanding the involvement of the hippocampus in memory [71]. Importantly, stress and CRH also affect the activity of these systems [72–74]

Notably, the NI is the source of an ascending GABAergic pathway to the SHS, and NI neurons display activity related to hippocampal theta rhythm in rats and mice [15, 19–21, 48, 64, 75]. Moreover, it has recently been shown that the NI plays a role in fear memory formation in mice via direct inhibition of the SST neurons of the hippocampus [21, 23]. This evidence confirmed earlier proposals, based on several studies in rodents, that demonstrated the involvement of the NI-RLN3/RXFP3 system in declarative and contextual memory [19, 27, 28, 75]. These recent studies employing optogenetics and viral-based pathway mapping revealed that the ascending arm of the NI-SHS pathway can regulate fear memory via effects on SST-positive interneurons in the hippocampus and on hippocampally-projecting septal neurons [21, 23], and that NI activity can be regulated by descending inputs from the prefrontal and retrosplenial cortex [23]. In this regard, earlier studies have reported that SST interneurons receive a RLN3 innervation and express RLN3 receptors (RXFP3 mRNA) [51, 76, 77].



Notably, the degeneration of GABA and somatostatin/GABA neurons occurs in the hippocampus and basal forebrain-cortical systems in AD and other neurodegenerative dementias [78]. Therefore, overactivity or degeneration of the inputs from the NI may have adverse consequences for memory formation and may be a target for neural dysregulation by AD pathological processes. In our initial studies, we observed an accumulation of RLN3-IR in a distinct population of neurons in the CA1, CA2, and DG layers of the human hippocampus. In the DG, RLN3-IR was present in neurons containing SST-IR, and this peptide ‘accumulation’ may be associated with the normal function or pathological dysfunction of the RLN3/RXFP3 system at different stages of aging or age-related pathology.

#### Possible impact of AD pathology on NI RLN3 neurons

Brainstem networks including those ascending from the LC and the raphe nuclei are highly susceptible to neurodegenerative diseases, including AD [79–82], and phosphorylated-tau has been used as a marker of neurodegeneration in diseases such as Alzheimer’s disease and related dementias (ADRD) [83–86]. Interestingly, phosphorylated-tau deposition was demonstrated at the level of the pons in cases diagnosed with AD [87, 88]. Pioneering studies by Braak and colleagues report that intracellular pretangles are first identified in the LC and various other brainstem nuclei, years before the presence of mature tangles in the limbic system [1]. Notably, we observed an accumulation of phosphorylated-tau (reflected by AT8-IR) in RLN3-containing neurons of the NI of a Braak IV AD subject, suggesting a possible association of the NI with AD etiology.

A likely role of NI and related circuits in memory formation [21, 40, 89], and evidence that tau accumulation induces synaptic and spatial memory impairment [90–92], highlight the importance of further characterizing the neurochemical anatomy of the human NI and the impact of AD on this profile.

#### Limitations of these studies

While studies of postmortem human brain tissue have provided valuable insights into the neurochemical profile of human NI neurons, it is important to acknowledge that this approach is not able to capture dynamic changes that occur in the brain of living individuals. In addition, sampling from hemi-brains may introduce some degree of bias, as it does not sample the complete bilateral NI. While efforts have been made to ensure accurate and representative sampling, future studies could consider accounting for potential differences between sampled hemi-brains and the complete bilateral NI.

Postmortem tissue from elderly patients presents neuronal loss therefore postmortem tissue from young adults would be beneficial to quantify the neuronal population in the NI. While free-floating formalin-fixed sections present a well conserved neuroanatomy, and low levels of autofluorescence, the availability of this specific type of tissue is limited. Comparative studies using larger sample sizes are warranted. Finally, all the subjects used in this study were Caucasian, which may limit the generalizability of our findings to other racial and ethnic backgrounds. It is important to recognize the potential influence of genetic and environmental factors that can vary across different populations and to address this limitation, future studies should include a more diverse cohort of subjects to ensure the broad applicability of results. Institutions that serve more diverse populations could assist the recruitment of participants from various racial and ethnic backgrounds.

#### Future experiments

Further characterization of the molecular profile of neurons within the human NI as a function of age and AD is warranted, and future studies should consider employing techniques that allow real-time monitoring of human NI activity, such as functional imaging methods [93]. Such approaches would provide a more comprehensive understanding of the temporal dynamics of human NI function as well as their cellular underpinnings.

#### Conclusions

The NI is an important, but understudied nucleus in the anterior pons of the human brain. RLN3 is a useful marker of the NI. Accumulation of phosphorylated-tau was detected in the NI of an AD patient. RLN3-IR was detected in a population of hippocampal neurons, in the absence of its corresponding mRNA. The involvement of the NI and related neural circuits in memory and ADRDs should be explored in future comparative studies using imaging and postmortem tissue.

#### Abbreviations

ACD	Advanced Cell Diagnostics
AD	Alzheimer’s disease
ADRC	Alzheimer’s Disease Research Center
ADRD	Alzheimer’s disease and related dementias
BDP	Brain Bank Donation Program
BSA	Bovine serum albumin
CCK	Cholecystokinin
CGM	Central gray of the medulla
CRH	Corticotrophin-releasing hormone
CRHR1	Corticotrophin-releasing hormone receptor-1
DAB	3,3’-diaminobenzidine
D2R	D2-like dopamine receptor
EP	Ependymal
GABA	γ-Aminobutyric acid
GAD	Glutamic acid decarboxylase
H&E	Hematoxylin and eosin
HG	Hypocellular gap
IHC	Immunohistochemistry

IR	Immunoreactivity
ISH	In situ hybridization
LC	Locus coeruleus
MAP2	Microtubule-associated protein-2
MCH	Melanin-concentrating hormone
MCH-1	Melanin-concentrating hormone receptor-1
mIf	Medial longitudinal fasciculus
NMB	Neuromedin-B
NI	Nucleus incertus
ON	Overnight
OX1	Orexin receptor-1
OX2	Orexin receptor-2
PAG	Periaqueductal gray
PBS	Phosphate-buffered saline
PBS-T	Phosphate-buffered saline with Tween® 20 detergent
PRn	Pontine raphe nucleus
RLN3	Relaxin-3
RT	Room temperature
RXFP3	Relaxin-family peptide-3 receptor
SHS	Septohippocampal system
SN	Substantia nigra
TBS-T	Tris-buffered saline with 0.1% Tween® 20 detergent
vGAT1	Vesicular GABA transporter-1
4V	Fourth ventricle
5-HT <sub>1A</sub>	Serotonin-1A receptor

## Supplementary Information

The online version contains supplementary material available at <https://doi.org/10.1186/s40659-024-00523-z>.

Additional file 1. Fig. 1. Specificity of RLN3 Antiserum Assessed in Human Testis. (A–C) RLN3-immunoreactivity (IR) detected in spermatozoa cells in the human testis; (B,C) Higher magnification images of RLN3-IR in boxed area in A. (D–F) Pre-adsorption of RLN3 antibody pre-incubated overnight with RLN3 recombinant peptide. (E,F) Higher magnification images of boxed area in D. Tissue counterstained with neutral red. (G) Positive dot-blot for RLN3 antiserum against native peptide; circular immunoreactivity in the center of the cellulose membrane reflects the binding of the peptide (RLN3) to the antibody (anti-RLN3).

Additional file 2. Fig. 2. Hematoxylin and Eosin Staining of Pons of Human Brain. (A) Low-power image of the neuroanatomy of the coronal pons containing the NI. (B) Higher magnification of the boxed area in A. (C) Higher magnification of the boxed area in B. (D) Higher magnification of the boxed area in C. Abbreviations: EP, ependyma, 4V, fourth ventricle, HG, Hypocellular gap, LC, locus coeruleus, mlf, medial longitudinal fasciculus, NI, nucleus incertus.

## Acknowledgements

The authors declare no competing financial interests. The authors are grateful to the Banner Sun Health Research Institute Brain and Body Donation Program of Sun City, Arizona for the provision of human biological materials. The authors would like to acknowledge Zerrin Uzum from the Biosciences Core Facilities at Arizona State University for her assistance in using the slide scanner and image processing.

## Author contributions

C.A. and A.L.G. conceived the study and designed the experiments. C.A., A.G., A.T., A.I., J.P., C.S., J.N., L.T., D.K., performed the experiments. C.A., D.F.M., G.E.S., T.G.B., A.B., A.C. and A.L.G. analyzed the data. D.F.M., T.G.B., G.E.S., A.B. and A.L.G. supervised the research. C.A. wrote the manuscript and prepared the figures, with editorial input from all the authors.

## Funding

The Brain and Body Donation Program is supported by the National Institute of Neurological Disorders and Stroke (U24 NS072026 National Brain and Tissue Resource for Parkinson's Disease and Related Disorders), the National Institute on Aging (P30 AG19610 Arizona Alzheimer's Disease Core Center), the Arizona Department of Health Services (contract 211002, Arizona Alzheimer's Research

Center), the Arizona Biomedical Research Commission (contracts 4001, 0011, 05-901 and 1001 to the Arizona Parkinson's Disease Consortium) and the Michael J. Fox Foundation for Parkinson's Research. The authors gratefully acknowledge grants from the Strategic Program Initiative of Excellence in the Jagiellonian University—Minigrant at the Faculty of Biology 2023 (A.G.), the National Science Centre, Poland (UMO-2023/49/B/NZ4/01885, A.B.), the BrightFocus Foundation (A2021006, C.A.), and the Alzheimer's Association (AARFD-22-972099, C.A.).

## Availability of data and materials

Not applicable.

## Declarations

### Ethics approval and consent to participate

Written informed consent for autopsy was obtained in compliance with the institutional guidelines of Banner Sun Health Research Institute. The Institutional Review Boards for Banner Sun Health Research Institute approved the operations of the Brain and Body Donation Program, including recruitment, enrollment, autopsy and sharing of biospecimens and data. In addition, samples were analyzed anonymously (e.g. sample numbers) throughout the experimental process.

### Consent for publication

Not applicable.

### Competing interests

All authors declare no competing interests.

### Author details

<sup>1</sup>Arizona State University-Banner Neurodegenerative Disease Research Center, Tempe, AZ, USA. <sup>2</sup>Department of Neurophysiology and Chronobiology, Institute of Zoology and Biomedical Research, Jagiellonian University, Krakow, Poland. <sup>3</sup>Arizona Alzheimer's Consortium, Phoenix, AZ, USA. <sup>4</sup>Banner Sun Health Research Institute, Sun City, AZ, USA. <sup>5</sup>Quebec Heart and Lung Institute, Quebec City, QC, Canada. <sup>6</sup>Department of Neuroscience, Mayo Clinic, Scottsdale, AZ, USA. <sup>7</sup>Faculty of Pharmacy, Université Laval, Quebec City, QC, Canada. <sup>8</sup>Florey Department of Neuroscience and Mental Health and Department of Anatomy and Physiology and The Florey Institute of Neuroscience and Mental Health, The University of Melbourne, Melbourne, VIC, Australia.

Received: 13 October 2023 Accepted: 7 June 2024

Published online: 16 July 2024

## References

- Braak H, Thal DR, Ghebremedhin E, Del Tredici K. Stages of the pathologic process in Alzheimer disease: age categories from 1 to 100 years. *J Neuro-pathol Exp Neurol*. 2011;70:960–9.
- Ehrenberg AJ, Kelberman MA, Liu KY, Dahl MJ, Weinschenker D, Falgas N, et al. Priorities for research on neuromodulatory subcortical systems in Alzheimer's disease: Position paper from the NSS PIA of ISTAART. *Alzheimers Dement*. 2023;19:2182–96.
- Betts MJ, Kirilina E, Otaduy MCG, Ivanov D, Acosta-Cabrero J, Callaghan MF, et al. Locus coeruleus imaging as a biomarker for noradrenergic dysfunction in neurodegenerative diseases. *Brain*. 2019;142:2558–71.
- Ehrenberg AJ, Nguy AK, Theofilas P, Dunlop S, Suemoto CK, Di Lorenzo Alho AT, et al. Quantifying the accretion of hyperphosphorylated tau in the locus coeruleus and dorsal raphe nucleus: the pathological building blocks of early Alzheimer's disease. *Neuropathol Appl Neurobiol*. 2017;43:393–408.
- Takeuchi T, Duszkiwicz AJ, Sonneborn A, Spooner PA, Yamasaki M, Watanabe M, et al. Locus coeruleus and dopaminergic consolidation of everyday memory. *Nature*. 2016;537:357–62.
- Kempadoo KA, Mosharov EV, Choi SJ, Sulzer D, Kandel ER. Dopamine release from the locus coeruleus to the dorsal hippocampus promotes spatial learning and memory. *Proc Natl Acad Sci U S A*. 2016;113:14835–40.

7. Sara SJ, Vankov A, Herve A. Locus coeruleus-evoked responses in behaving rats: a clue to the role of noradrenaline in memory. *Brain Res Bull.* 1994;35:457–65.
8. Streeter GL. Anatomy of the floor of the fourth ventricle. *Am J Anat.* 1903;2:299–313.
9. Castaldi L. Studi sulla struttura e sullo sviluppo del mesencefalo. *Arch Ital Anat Embriol.* 1923;20:23–225.
10. Chatfield PO, Lyman CP. An unusual structure in the floor of the fourth ventricle of the golden hamster. *Mesocricetus auratus* *J Comp Neurol.* 1954;101:225–35.
11. Berman AL. The brain stem of the cat: a cytoarchitectonic atlas with stereotaxic coordinates. Seattle: UW Press; 1968.
12. Paxinos G, Watson C. The rat brain in stereotaxic coordinates. 6th ed. Amsterdam: Boston Academic Press/Elsevier; 2007.
13. Ford B, Holmes CJ, Mainville L, Jones BE. GABAergic neurons in the rat pontomesencephalic tegmentum: Codistribution with cholinergic and other tegmental neurons projecting to the posterior lateral hypothalamus. *J Comp Neurol.* 1995;363:177–96.
14. Szlaga A, Sambak P, Trenk A, Gugula A, Singleton CE, Drwiega G, et al. Functional neuroanatomy of the rat nucleus incertus-medial septum tract: Implications for the cell-specific control of the septohippocampal pathway. *Front Cell Neurosci.* 2022;16:836116.
15. Gil-Miravet I, Nunez-Molina A, Navarro-Sanchez M, Castillo-Gomez E, Ros-Bernal F, Gundlach AL, et al. Nucleus incertus projections to rat medial septum and entorhinal cortex: rare collateralization and septal-gating of temporal lobe theta rhythm activity. *Brain Struct Funct.* 2023;228:1307–28.
16. Garcia-Diaz C, Gil-Miravet I, Albert-Gasco H, Manas-Ojeda A, Ros-Bernal F, Castillo-Gomez E, et al. Relaxin-3 innervation from the nucleus incertus to the parahippocampal cortex of the rat. *Front Neuroanat.* 2021;15:674649.
17. Goto M, Swanson LW, Canteras NS. Connections of the nucleus incertus. *J Comp Neurol.* 2001;438:86–122.
18. Olucha-Bordonau FE, Teruel V, Barcia-Gonzalez J, Ruiz-Torner A, Valverde-Navarro AA, Martinez-Soriano F. Cytoarchitecture and efferent projections of the nucleus incertus of the rat. *J Comp Neurol.* 2003;464:62–97.
19. Ryan PJ, Ma S, Olucha-Bordonau FE, Gundlach AL. Nucleus incertus—an emerging modulatory role in arousal, stress and memory. *Neurosci Biobehav.* 2011;35:1326–41.
20. Lu L, Ren Y, Yu T, Liu Z, Wang S, Tan L, et al. Control of locomotor speed, arousal, and hippocampal theta rhythms by the nucleus incertus. *Nat Commun.* 2020;11:262.
21. Szőnyi A, Sos KE, Nyilas R, Schlingloff D, Domonkos A, Takács VT, et al. Brainstem nucleus incertus controls contextual memory formation. *Science.* 2019;364:eaaw0445.
22. Nasirova N, Quina LA, Morton G, Walker A, Turner EE. Mapping cell types and efferent pathways in the ascending relaxin-3 system of the nucleus incertus. *eNeuro.* 2020;7:0272.
23. Zicho K, Sos KE, Papp P, Barth AM, Misak E, Orosz A, et al. Fear memory recall involves hippocampal somatostatin interneurons. *PLoS Biol.* 2023;21:e3002154.
24. Smith CM, Shen PJ, Banerjee A, Bonaventure P, Ma S, Bathgate RA, et al. Distribution of relaxin-3 and RXFP3 within arousal, stress, affective, and cognitive circuits of mouse brain. *J Comp Neurol.* 2010;518:4016–45.
25. Donizetti A, Grossi M, Pariante P, D'Aniello E, Izzo G, Minucci S, et al. Two neuron clusters in the stem of postembryonic zebrafish brain specifically express relaxin-3 gene: First evidence of nucleus incertus in fish. *Dev Dyn.* 2008;237:3864–9.
26. Ma S, Sang Q, Lanciego JL, Gundlach AL. Localization of relaxin-3 in brain of *Macaca fascicularis*: identification of a nucleus incertus in primate. *J Comp Neurol.* 2009;517:856–72.
27. Nategh M, Nikseresh S, Khodaghohi F, Motamedi F. Nucleus incertus inactivation impairs spatial learning and memory in rats. *Physiol Behav.* 2015;139:112–20.
28. Albert-Gasco H, Garcia-Aviles A, Moustafa S, Sanchez-Sarasua S, Gundlach AL, Olucha-Bordonau FE, et al. Central relaxin-3 receptor (RXFP3) activation increases ERK phosphorylation in septal cholinergic neurons and impairs spatial working memory. *Brain Struct Funct.* 2017;222:449–63.
29. Sanchez-Perez AM, Arnal-Vicente I, Santos FN, Pereira CW, ElMilili N, Sanjuan J, et al. Septal projections to nucleus incertus in the rat: Bidirectional pathways for modulation of hippocampal function. *J Comp Neurol.* 2015;523:565–88.
30. Trenk A, Walczak M, Szlaga A, Pradel K, Blasiak A, Blasiak T. Bidirectional communication between the pontine nucleus incertus and the medial septum is carried out by electrophysiologically-Distinct neuronal populations. *J Neurosci.* 2022;42:2234–52.
31. Mesulam M, Shaw P, Mash D, Weintraub S. Cholinergic nucleus basalis tauopathy emerges early in the aging-MCI-AD continuum. *Ann Neurol.* 2004;55:815–28.
32. Spiegel AM, Koh MT, Vogt NM, Rapp PR, Gallagher M. Hilar interneuron vulnerability distinguishes aged rats with memory impairment. *J Comp Neurol.* 2013;521:3508–23.
33. Ma S, Bonaventure P, Ferraro T, Shen PJ, Burazin TC, Bathgate RA, et al. Relaxin-3 in GABA projection neurons of nucleus incertus suggests widespread influence on forebrain circuits via G-protein-coupled receptor-135 in the rat. *Neuroscience.* 2007;144:165–90.
34. Tanaka M, Iijima N, Miyamoto Y, Fukusumi S, Itoh Y, Ozawa H, et al. Neurons expressing relaxin 3/INSL 7 in the nucleus incertus respond to stress. *Eur J Neurosci.* 2005;21:1659–70.
35. Bathgate RA, Samuel CS, Burazin TC, Layfield S, Claasz AA, Reytomas IG, et al. Human relaxin gene 3 (H3) and the equivalent mouse relaxin (M3) gene. Novel members of the relaxin peptide family. *J Biol Chem.* 2002;277:1148–57.
36. Burazin TC, Bathgate RA, Macris M, Layfield S, Gundlach AL, Tregear GW. Restricted, but abundant, expression of the novel rat gene-3 (R3) relaxin in the dorsal tegmental region of brain. *J Neurochem.* 2002;82:1553–7.
37. Ma S, Smith CM, Blasiak A, Gundlach AL. Distribution, physiology and pharmacology of relaxin-3/RXFP3 systems in brain. *Br J Pharmacol.* 2017;174:1034–48.
38. Liu C, Eriste E, Sutton S, Chen J, Roland B, Kuei C, et al. Identification of relaxin-3/INSL7 as an endogenous ligand for the orphan G-protein-coupled receptor GPCR135. *J Biol Chem.* 2003;278:50754–64.
39. Leyens H, Walter D, Clauwaert L, Hellemans L, van Gastel J, Vasudevan L, et al. The relaxin-3 receptor, RXFP3, is a modulator of aging-related disease. *Int J Mol Sci.* 2022;23:4387.
40. Gil-Miravet I, Manas-Ojeda A, Ros-Bernal F, Castillo-Gomez E, Albert-Gasco H, Gundlach AL, et al. Involvement of the nucleus incertus and relaxin-3/RXFP3 signaling system in explicit and implicit memory. *Front Neuroanat.* 2021;15:637922.
41. Calvez J, de Avila C, Guevremont G, Timofeeva E. Stress differentially regulates brain expression of corticotropin-releasing factor in binge-like eating prone and resistant female rats. *Appetite.* 2016;107:585–95.
42. Calvez J, de Avila C, Matte LO, Guevremont G, Gundlach AL, Timofeeva E. Role of relaxin-3/RXFP3 system in stress-induced binge-like eating in female rats. *Neuropharmacology.* 2016;102:207–15.
43. Banerjee A, Shen PJ, Ma S, Bathgate RA, Gundlach AL. Swim stress excitation of nucleus incertus and rapid induction of relaxin-3 expression via CRF1 activation. *Neuropharmacology.* 2010;58:145–55.
44. Beach TG, Adler CH, Sue LI, Serrano G, Shill HA, Walker DG, et al. Arizona study of aging and neurodegenerative disorders and Brain and body donation program. *Neuropathology.* 2015;35:354–89.
45. Schneider CA, Rasband WS, Eliceiri KW. NIH Image to ImageJ: 25 years of image analysis. *Nat Methods.* 2012;9:671–5.
46. Hanafy S, Sabry JH, Akl EM, Elethy RA, Mostafa T. Serum relaxin-3 hormone relationship to male delayed puberty. *Andrologia.* 2018;50:e12882.
47. Dehmelt L, Halpain S. The MAP2/Tau family of microtubule-associated proteins. *Genome Biol.* 2005;6:204.
48. Ma S, Blasiak A, Olucha-Bordonau FE, Verberne AJ, Gundlach AL. Heterogeneous responses of nucleus incertus neurons to corticotrophin-releasing factor and coherent activity with hippocampal theta rhythm in the rat. *J Physiol.* 2013;591:3981–4001.
49. Olucha-Bordonau FE, Albert-Gasco H, Ros-Bernal F, Rytova V, Ong-Palsson EKE, Ma S, et al. Modulation of forebrain function by nucleus incertus and relaxin-3/RXFP3 signaling. *CNS Neurosci Ther.* 2018;24:694–702.
50. Ma S, Gundlach AL. Relaxin-family peptide and receptor systems in brain: insights from recent anatomical and functional studies. *Adv Exp Med Biol.* 2007;612:119–37.
51. Haidar M, Tin K, Zhang C, Nategh M, Covita J, Wykes AD, et al. Septal GABA and glutamate neurons express RXFP3 mRNA and depletion of septal RXFP3 impaired spatial search strategy and long-term reference memory in adult mice. *Front Neuroanat.* 2019;8(13):30.
52. Kubota Y, Inagaki S, Shiosaka S, Cho HJ, Tateishi K, Hashimura E, et al. The distribution of cholecystokinin octapeptide-like structures in the lower



- brain stem of the rat: An immunohistochemical analysis. *Neuroscience*. 1983;9:587–604.
53. Ohki-Hamazaki H. Neuromedin B. *Prog Neurobiol*. 2000;62:297–312.
  54. Blasiak A, Siwiec M, Grabowiecka A, Blasiak T, Czerw A, Blasiak E, et al. Excitatory orexinergic innervation of rat nucleus incertus—Implications for ascending arousal, motivation and feeding control. *Neuropharmacology*. 2015;99:432–47.
  55. Kastman HE, Blasiak A, Walker L, Siwiec M, Krstew EV, Gundlach AL, et al. Nucleus incertus Orexin2 receptors mediate alcohol seeking in rats. *Neuropharmacology*. 2016;110(Pt A):82–91.
  56. Sabetghadam A, Grabowiecka-Nowak A, Kania A, Gugula A, Blasiak E, Blasiak T, et al. Melanin-concentrating hormone and orexin systems in rat nucleus incertus: dual innervation, bidirectional effects on neuron activity, and differential influences on arousal and feeding. *Neuropharmacology*. 2018;139:238–56.
  57. Greco MA, Shiromani PJ. Hypocretin receptor protein and mRNA expression in the dorsolateral pons of rats. *Brain Res Mol Brain Res*. 2001;88:176–82.
  58. Ma S, Hangya B, Leonard CS, Wisden W, Gundlach AL. Dual-transmitter systems regulating arousal, attention, learning and memory. *Neurosci Biobehav Rev*. 2018;85:21–33.
  59. Miyamoto Y, Watanabe Y, Tanaka M. Developmental expression and serotonergic regulation of relaxin 3/INSL7 in the nucleus incertus of rat brain. *Regul Pept*. 2008;145:54–9.
  60. Kumar JR, Rajkumar R, Farooq U, Lee LC, Tan FC, Dawe GS. Evidence of D2 receptor expression in the nucleus incertus of the rat. *Physiol Behav*. 2015;151:525–34.
  61. Kumar JR, Rajkumar R, Lee LC, Dawe GS. Nucleus incertus contributes to an anxiogenic effect of buspirone in rats: Involvement of 5-HT1A receptors. *Neuropharmacology*. 2016;110:1–14.
  62. Kumar JR, Rajkumar R, Jayakody T, Marwari S, Hong JM, Ma S, et al. Relaxin in the brain: a case for targeting the nucleus incertus network and relaxin-3/RXFP3 system in neuropsychiatric disorders. *Br J Pharmacol*. 2017;174:1061–76.
  63. Schwabe L, Joels M, Roozendaal B, Wolf OT, Oitzl MS. Stress effects on memory: an update and integration. *Neurosci Biobehav Rev*. 2012;36:1740–9.
  64. Schott AL, Baik J, Chung S, Weber F. A medullary hub for controlling REM sleep and pontine waves. *Nat Commun*. 2023;14:3922.
  65. Lesch K-P, Waider J. Serotonin in the modulation of neural plasticity and networks: implications for neurodevelopmental disorders. *Neuron*. 2012;76:175–91.
  66. Woolf NJ, Butcher LL. Cholinergic systems mediate action from movement to higher consciousness. *Behav Brain Res*. 2011;221:488–98.
  67. Smith CM, Walker AW, Hosken IT, Chua BE, Zhang C, Haidar M, et al. Relaxin-3/RXFP3 networks: an emerging target for the treatment of depression and other neuropsychiatric diseases? *Front Pharmacol*. 2014;5:46.
  68. Haam J, Yakel JL. Cholinergic modulation of the hippocampal region and memory function. *J Neurochem*. 2017;142:111–21.
  69. Mather M, Clewett D, Sakaki M, Harley CW. Norepinephrine ignites local hotspots of neuronal excitation: How arousal amplifies selectivity in perception and memory. *Behav Brain Res*. 2016;39:e200.
  70. Smith GS, Barrett FS, Joo JH, Nassery N, Savonenko A, Sodums DJ, et al. Molecular imaging of serotonin degeneration in mild cognitive impairment. *Neurobiol Dis*. 2017;37:33–41.
  71. Sara SJ. The locus coeruleus and noradrenergic modulation of cognition. *Nat Rev Neurosci*. 2009;10:211–23.
  72. Chaouloff F. Serotonin, stress and corticoids. *J Psychopharmacol*. 2000;14:139–51.
  73. Gilad GM. The stress-induced response of the septo-hippocampal cholinergic system. A vectorial outcome of psychoneuroendocrinological interactions. *Psychoneuroendocrinology*. 1987;12:167–84.
  74. Valentino RJ, Van Bockstaele E. Convergent regulation of locus coeruleus activity as an adaptive response to stress. *Eur J Pharmacol*. 2008;583:194–203.
  75. Ma S, Olucha-Bordonau FE, Hossain MA, Lin F, Kuei C, Liu C, et al. Modulation of hippocampal theta oscillations and spatial memory by relaxin-3 neurons of the nucleus incertus. *Learn Mem*. 2009;16:730–42.
  76. Haidar M, Guèvremont G, Zhang C, Bathgate R, Timofeeva E, Smith CM, et al. Relaxin-3 inputs target hippocampal interneurons and deletion of hilar relaxin-3 receptors in “floxed-RXFP3” mice impairs spatial memory. *Hippocampus*. 2017;27:529–46.
  77. Rytova V, Ganella DE, Hawkes D, Bathgate RA, Ma S, Gundlach AL. Chronic activation of the relaxin-3 receptor on GABA neurons in rat ventral hippocampus promotes anxiety and social avoidance. *Hippocampus*. 2019;29:905–20.
  78. Rozycka A, Liguz-Lecznar M. The space where aging acts: focus on the GABAergic synapse. *Aging Cell*. 2017;16:634–43.
  79. Rorabaugh JM, Chalermpananupap T, Botz-Zapp CA, Fu VM, Lembeck NA, Cohen RM, et al. Chemogenetic locus coeruleus activation restores reversal learning in a rat model of Alzheimer’s disease. *Brain*. 2017;140:3023–38.
  80. Fortress AM, Hamlett ED, Vazey EM, Aston-Jones G, Cass WA, Boger HA, et al. Designer receptors enhance memory in a mouse model of Down syndrome. *J Neurosci*. 2015;35:1343–53.
  81. Hamlett ED, Ledreux A, Gilmore A, Vazey EM, Aston-Jones G, Boger HA, et al. Inhibitory designer receptors aggravate memory loss in a mouse model of down syndrome. *Neurobiol Dis*. 2020;134:104616.
  82. Shine JM, Breakspear M, Bell PT, Ehgoetz Martens KA, Shine R, Koyejo O, et al. Human cognition involves the dynamic integration of neural activity and neuromodulatory systems. *Nat Neurosci*. 2019;22:289–96.
  83. Blennow K, Wallin A, Agren H, Spenger C, Siegfried J, Vanmechelen E. Tau protein in cerebrospinal fluid: a biochemical marker for axonal degeneration in Alzheimer disease? *Mol Chem Neurobiol*. 1995;26:231–45.
  84. Mandelkow EM, Mandelkow E. Tau as a marker for Alzheimer’s disease. *Trends Biochem Sci*. 1993;18:480–3.
  85. Buee L, Bussiere T, Buee-Scherrer V, Delacourte A, Hof PR. Tau protein isoforms, phosphorylation and role in neurodegenerative disorders. *Brain Res Rev*. 2000;33:95–130.
  86. Hampel H, Buerger K, Zinkowski R, Teipel SJ, Goernitz A, Andreasen N, et al. Measurement of phosphorylated tau epitopes in the differential diagnosis of Alzheimer disease: a comparative cerebrospinal fluid study. *Arch Gen Psychiatry*. 2004;61:95–102.
  87. Uematsu M, Nakamura A, Ebashi M, Hirokawa K, Takahashi R, Uchihara T. Brainstem tau pathology in Alzheimer’s disease is characterized by increase of three repeat tau and independent of amyloid beta. *Acta Neuropathol Commun*. 2018;6:1.
  88. Rub U, Stratmann K, Heinsen H, Turco DD, Seidel K, Dunnen W, et al. The brainstem tau cytoskeletal pathology of Alzheimer’s disease: a brief historical overview and description of its anatomical distribution pattern, evolutionary features, pathogenetic and clinical relevance. *Curr Alzheimer Res*. 2016;13:1178–97.
  89. Takacs V, Bardoczi Z, Orosz A, Major A, Tar L, Berki P, et al. Synaptic and dendritic architecture of different types of hippocampal somatostatin interneurons. *PLoS Biol*. 2024;22:e3002539.
  90. Biundo F, Del Prete D, Zhang H, Arancio O, D’Adamo L. A role for tau in learning, memory and synaptic plasticity. *Sci Rep*. 2018;8:3184.
  91. Wu M, Zhang M, Yin X, Chen K, Hu Z, Zhou Q, et al. The role of pathological tau in synaptic dysfunction in Alzheimer’s diseases. *Transl Neurodegener*. 2021;10:45.
  92. LaFerla FM, Oddo S. Alzheimer’s disease: Abeta, tau and synaptic dysfunction. *Trends Mol Med*. 2005;11:170–6.
  93. Veréb D, Mijalkov M, Canal-García A, Chang Y-W, Gomez-Ruis E, Gerboles BZ et al. Age-related differences in the functional topography of the locus coeruleus: implications for cognitive and affective functions. *medRxiv*. 2023.
  94. Johnson GV, Jope RS. The role of microtubule-associated protein 2 (MAP-2) in neuronal growth, plasticity, and degeneration. *J Neurosci Res*. 1992;33:505–12.

## Publisher’s Note

Springer Nature remains neutral with regard to jurisdictional claims in published maps and institutional affiliations.